RESEARCH ARTICLE
doi: 10.2306/scienceasia1513-1874.2026.037

ScienceAsia 52 (2): 2026: ID 2026037: **1–12**

Hawthorn flavonoids ameliorate NAFLD in mice: Association with enhanced gut butyrate production and hepatic PI3K/Akt signaling activation

Wei Chen[a,†], **Li Li**[b,†], **Xueyun Dong**[c], **Hao Xu**[c], **Changhe Zheng**[a], **Bo Zhang**[a], **Wenying Lu**[a], **Xin Ma**[d], **Na Li**[e], **Wen Xia**[f], **Asmaa Ali**[c,g], **Liang Wu**[c,*], **Yanxia Chen**[h,*]

[a] Department of Laboratory Medicine, Yancheng Tinghu District People's Hospital, Yancheng, Jiangsu 224001 China
[b] Department of Clinical Laboratory, Binhai County People's Hospital, Yancheng, Jiangsu 224500 China
[c] Department of Laboratory Medicine, School of Medicine, Jiangsu University, Jiangsu 212013 China
[d] Department of Critical Care Medicine, Jurong Hospital, Affiliated to Jiangsu University, Jiangsu 212400 China
[e] Department of Clinical Laboratory, Affiliated Women's Hospital of Jiangnan University, Wuxi 214000 China
[f] School of Pharmaceutical and Chemical Technology, Zhenjiang College, Zhenjiang 212028 China
[g] Department of Pulmonary Medicine, Abbassia Chest Hospital, EMOH, Cairo 11517 Egypt
[h] Department of Orthopedics, Zhenjiang Hospital Affiliated to Nanjing University of Chinese Medicine (Zhenjiang Hospital of Traditional Chinese Medicine), Zhenjiang 212003 China

*Corresponding authors, e-mail: cyx13861352591@163.com, wl_ujs@163.com
† These authors contributed equally to this work.

Received 23 Jan 2026, Accepted 12 Apr 2026
Available online 5 May 2026

ABSTRACT: Gut dysbiosis and disrupted gut-liver crosstalk drive non-alcoholic fatty liver disease (NAFLD), a global health burden intertwined with obesity and insulin resistance. This study investigated the therapeutic potential of Hawthorn flavonoid extract (HF) from *Crataegus* species in NAFLD management, focusing on its modulation of gut microbiota and metabolic pathways. Using a high-fat diet-induced NAFLD mouse model, 12-week HF supplementation (100 mg/kg/day) was administered. We evaluated therapeutic effects via hepatic steatosis, systemic insulin resistance, antioxidant capacity (SOD, GSH-Px, and MDA), and liver histology. Mechanistic insights were gained through gut microbiota composition, fecal butyrate, hepatic PI3K/Akt activation, and serum metabolomics. HF significantly attenuated hepatic steatosis, improved insulin sensitivity ($p < 0.05$), and restored antioxidant capacity by elevating SOD/GSH-Px activity and suppressing lipid peroxidation (MDA). Histology confirmed reduced hepatic lipid accumulation and inflammation. Furthermore, HF favorably altered gut microbial composition, enriching beneficial genera such as *Akkermansia* and *Bacteroides*, and increased colonic butyrate production. This microbial shift correlated with hepatic PI3K/Akt pathway activation ($p < 0.05$). Serum metabolomics identified HF-mediated reprogramming of taurine metabolism, glutathione recycling, and glycerophospholipid dynamics. In conclusion, HF alleviates NAFLD progression by restoring gut microbial ecology, enhancing butyrate production, and activating hepatic PI3K/Akt signaling, collectively modulating oxidative stress and lipid metabolism.

KEYWORDS: non-alcoholic fatty liver disease, Hawthorn flavonoids, butyrate, PI3K/Akt pathway, oxidative stress, gut microbiota

INTRODUCTION

NAFLD is a chronic liver disease characterized by excessive triglyceride accumulation within hepatocytes, affecting a substantial proportion of individuals with obesity, type 2 diabetes, or insulin resistance [1]. In the majority of patients, NAFLD follows a progressive course, potentially advancing to non-alcoholic steatohepatitis (NASH), which may further lead to liver fibrosis, cirrhosis, and hepatocellular carcinoma. It has become a major public health burden globally; for instance, its prevalence among adults in China is approximately 27.0% [2]. Although genetic predisposition, dietary patterns, and chronic inflammation are recognized contributors to NAFLD pathogenesis, the underlying mechanisms remain incompletely elucidated, and targeted therapeutic options are still limited.

Current evidence indicates that dyslipidemia, chronic inflammation, and oxidative stress represent central drivers in the initiation and progression of NAFLD. Insulin resistance disrupts systemic lipid homeostasis, promoting ectopic lipid deposition in the liver—an early step in hepatic injury [3]. This lipid overload exacerbates mitochondrial dysfunction and reactive oxygen species generation, inducing oxidative damage and activating pro-inflammatory signaling pathways. Sustained hepatic inflammation and oxidative stress promote activation of hepatic stellate cells, leading to extracellular matrix deposition and fibrosis [4]. Therefore, therapeutic strategies aimed at mitigating inflammation and oxidative stress are considered promising for slowing NAFLD progression.

Emerging research underscores the gut–liver axis as a critical interface in NAFLD pathophysiology. Dysbiosis of the gut microbiota can compromise intesti-

nal barrier integrity, facilitating the translocation of bacteria and pathogen-associated molecular patterns into the portal circulation [5]. This process triggers systemic and hepatic inflammation, as well as oxidative stress, ultimately promoting steatosis and hepatocellular injury. Consequently, modulating the gut microbial ecosystem has emerged as a promising therapeutic direction for NAFLD [6]. Within this strategic framework, natural polyphenols derived from plants, particularly flavonoids, are considered potential intervention candidates due to their widely reported multi-target bioactivities, including anti-inflammatory, antioxidant [7], and gut microbiota-modulating properties [8]. Notably, flavonoids from the traditional medicinal plant hawthorn (*Crataegus* spp.) have demonstrated significant efficacy in these aspects, highlighting their potential application in NAFLD management [9]. However, the specific interventions and mechanisms by which Hawthorn flavonoids influence NAFLD via the gut–liver axis remain inadequately elucidated, warranting further investigation.

In recent years, it has been discovered that many traditional Chinese herbs exhibit therapeutic effects on NAFLD, primarily attributed to their complex anti-inflammatory and antioxidant components [10]. In the current context where effective drugs for NAFLD treatment remain scarce, the exploration and screening of various lead compounds from traditional Chinese herbs for further in-depth research are of great significance. Hawthorn, a commonly used traditional Chinese herb, is often employed in the treatment of NAFLD [11]. Hawthorn flavonoids (HF), the most important active compounds in hawthorn, have been found to alleviate hepatic steatosis, insulin resistance, and endoplasmic reticulum stress, thereby contributing to the improvement of NAFLD symptoms [12]. Furthermore, emerging evidence suggests that the therapeutic effects of HF on metabolic diseases are closely associated with the modulation of gut microbiota [13]. However, there is currently a lack of direct research on the mechanism of oral Hawthorn flavonoids in the treatment of NAFLD specifically through gut microbiota regulation. Therefore, this study aims to investigate the regulatory effects of HF on the gut microbiota in NAFLD mice.

MATERIALS AND METHODS

Animals and experimental design

Male ICR mice (22 ± 4 g) were obtained from Nanjing Wukong Biotechnology Co., Ltd. (Nanjing, China) and housed under standard conditions in the Experimental Animal Center of Jiangsu University. This strain was selected for its established susceptibility to diet-induced metabolic disorders and its frequent use in nutritional intervention studies. After one week of acclimatization, the mice were randomly assigned into three groups ($n = 6$ per group): a normal control group fed a standard chow diet (NC), a high-fat diet-induced NAFLD model group (NAFLD), and a Hawthorn flavonoid intervention group (HF). Mice in the NAFLD and HF groups were fed a high-fat diet (D12109C, Beijing Future Biotech Co., Ltd., Beijing, China) with the following composition (w/w): 20% fat (primarily lard and soybean oil, providing 40% of kcal), 1.125% cholesterol, 0.45% sodium cholate, 20% protein, and 50% carbohydrates, supplemented with fiber, vitamins, and minerals. This diet is widely used to induce NAFLD features including steatosis and insulin resistance [14]. All animals had free access to sterile purified water throughout the 12-week study period, and the NAFLD model was established as previously described.

The HF extract was purchased from Shanghai Duma Biotechnology Co., Ltd. (Shanghai, China). According to the manufacturer's technical data and Certificate of Analysis (COA), the extract was standardized to contain not less than 60% total flavonoids as determined by UV-Vis spectrophotometry using rutin as a reference standard. Furthermore, the manufacturer's HPLC-DAD-MS analysis revealed that its major constituents were hyperoside ($\geqslant$15%), vitexin ($\geqslant$10%), rutin ($\geqslant$5%), and epicatechin. Since this was a commercially standardized product specifically enriched for flavonoids, the exact percentage of residual polysaccharides was not specified by the manufacturer and was not re-evaluated in our laboratory. The HF intervention dose was set at 100 mg/kg/day, corresponding to an approximate daily intake of 1.5 mg of total flavonoids per mouse (assuming 60% flavonoid content). This specific dosage was determined based on a combination of previously reported efficacious doses of HF in rodent NAFLD models [15] and our preliminary dose-finding experiments. The effective daily intake of 1.5 mg of pure flavonoids per mouse was calculated based on the administration of 100 mg/kg/day of the HF extract, an average mouse body weight of 25 g, and a standardized flavonoid extract purity of $\geqslant$60% (i.e., 100 mg/kg/day $\times$ 0.025 kg/mouse $\times$ 0.60 = 1.5 mg/day/mouse). In our preliminary study, this dose was deemed optimal and sufficient, as it significantly ameliorated core hepatic lipid accumulation and metabolic disturbances without inducing observable toxicity. Although it may not fully restore all NAFLD pathological markers to the basal levels of healthy controls, it provides an ideal window to investigate the underlying protective mechanisms.

To better mimic the clinical pathogenesis of metabolic diseases and evaluate the therapeutic—rather than strictly prophylactic—efficacy of HF, we adopted a sequential treatment paradigm. Mice were initially subjected to a 4-week HFD feeding regimen to induce early metabolic disturbances, characterized by significant body weight gain and the onset of insulin resistance. During this induction phase, body weight was closely monitored as the primary non-invasive

physiological indicator to confirm the successful establishment of the obesity phenotype in the HFD-fed mice relative to the NC group. Following the 4-week induction period (from week 5 to the end of week 12), daily oral gavage was initiated. Mice in the HF treatment group were administered the HF solution (prepared in 200 µl of normal saline), whereas mice in both the NC and NAFLD vehicle groups received an equal volume (200 µl) of normal saline.

At the termination of the experiment, all mice were euthanized under deep anesthesia induced by sevoflurane inhalation. All biological specimens, including blood samples, colonic contents, and liver tissues, were immediately collected. To ensure the accuracy of biochemical assays and prevent ongoing cellular glycolysis, the collected whole blood was allowed to clot at room temperature for 30 min and was promptly centrifuged at 3,000 × *g* for 10 min at 4 °C. The supernatant serum was immediately separated from the erythrocytes. The fractionated serum, along with the snap-frozen colonic contents and liver tissues, was then preserved at −80 °C for subsequent biochemical, metabolomic, and gut microbiota analyses.

Quantitative real-time PCR (qPCR) analysis

The mRNA expression levels of key inflammation-related factors and the bile acid synthesis rate-limiting enzyme CYP7A1 in liver tissues were quantified by reverse transcription quantitative real-time PCR (RT-qPCR). All gene-specific primers were designed and synthesized by GENEWIZ (Suzhou, China), as listed in Table S1.

Liver tissue samples were homogenized, and total RNA was purified using a commercial extraction kit (Vazyme, Cat. No. R4111-01, Nanjing, China) according to the manufacturer's protocol. RNA integrity was verified by assessing optical density ratios (A260/A280). Reverse transcription was performed on 1 µg of total RNA using a first-strand cDNA synthesis kit (Vazyme, Cat. No. R223-01) with oligo(dT) priming. For qPCR analysis, reactions (20 µl) were prepared containing a SYBR Green master mix (AceQ Universal, Vazyme, Cat. No. Q111-02), gene-specific primers (0.4 µl each, 10 µM), and cDNA template (10% of total volume). Amplification was carried out under standardized cycling conditions: initial denaturation (95 °C, 5 min), followed by 40 cycles of denaturation (95 °C, 3 s), annealing (58 °C, 20 s), and extension (72 °C, 30 s). Post-amplification melt curve analysis confirmed primer specificity. Target gene expression levels were normalized to β-actin and quantified using the $2^{-\Delta\Delta Ct}$ method.

Assessment of serum biomarkers and fecal short-chain fatty acids

Serum samples were thawed under controlled conditions (4 °C) and analyzed for metabolic and oxidative stress markers, including triglycerides (TG, Cat. No. A110-1-1), total cholesterol (TC, Cat. No. A111-1-1), malondialdehyde (MDA, Cat. No. A003-1-1), superoxide dismutase (SOD, Cat. No. A001-1-1), total antioxidant capacity (T-AOC, Cat. No. A015-1-1), reduced glutathione (GSH, Cat. No. A006-1-1), glucose (GLU, hexokinase assay, Cat. No. A154-1-1), and insulin (ELISA assay, Cat. No. H153-1-1), using commercially available assay kits (Nanjing Jiancheng Bioengineering Institute, Nanjing, China) following the manufacturer's instructions. Additionally, fecal butyrate levels were quantified by the Zhenjiang Center for Disease Control and Prevention (China) using ultra-performance liquid chromatography–quadrupole time-of-flight mass spectrometry (UPLC-QTOF-MS) [16].

Hepatic tissue morphological analysis

Liver specimens (∼2 mm^3) were preserved in 4% paraformaldehyde solution overnight at 4 °C, sequentially dehydrated through graded ethanol series, paraffin-embedded, and sliced into 4-µm sections using standard histotechnical procedures at Jiangsu University Affiliated Hospital's pathology facility. To characterize hepatic lipid deposition, cryopreserved tissue sections were processed with Oil Red O staining reagent (Beyotime Biotechnology, Cat. No. C0158M, Shanghai, China) following established protocols for neutral lipid detection. Parallel paraffin sections underwent conventional hematoxylin-eosin staining for comprehensive histological evaluation. Microstructural features and steatotic changes were systematically documented using bright-field microscopy (Nikon Instruments Inc., Melville, NY, USA).

Protein expression profiling by immunoblotting

Liver tissue fragments (200 mg) were rapidly homogenized in ice-cold RIPA buffer (Beyotime Biotechnology, Cat. No. P0013B) containing protease/phosphatase inhibitors using intermittent grinding cycles (15 s on/10 s off, 1 min total). Following centrifugation (12,000 × *g*, 15 min, 4 °C), the supernatant protein concentration was measured using BCA assay (Beyotime Biotechnology; Cat. No. P0012S). Samples were mixed with SDS-PAGE loading buffer and denatured (100 °C, 10 min), and equal protein amounts were resolved electrophoretically before transfer to PVDF membranes (Boster Biological Technology, Cat. No. PB0101, Wuhan, China). After milk-based blocking, membranes were probed overnight (4 °C) with primary antibodies against PI3K signaling components (Proteintech, Wuhan, China; PI3K/p-PI3K, Akt/p-Akt: 1:500; β-actin: 1:10,000). Signal detection was achieved through HRP-conjugated secondary antibody incubation (Beyotime Biotechnology; 1h, RT) and ECL substrate (Vazyme, Cat. No. E111-01), with band quantification performed using ImageJ software. Detailed information regarding all antibodies used in this study, including their specific catalog numbers and

Research Resource Identifiers (RRIDs), is summarized in Table S2.

Gut microbiome profiling via 16S rRNA sequencing

Fresh colonic specimens were cryopreserved in liquid nitrogen following collection and maintained at −80 °C prior to processing. Bacterial DNA underwent targeted amplification of the V3-V4 hypervariable regions before sequencing on Illumina MiSeq instruments performed by Ekemo Tech Group (Shenzhen, China). Bioinformatics analysis commenced with QIIME2 pipeline preprocessing (v2023.5), incorporating DADA2-based denoising for amplicon sequence variant determination and SILVA database (v138) alignment for taxonomic classification [17]. Microbial population characteristics were evaluated through α-diversity metrics and β-diversity comparisons among experimental cohorts.

Comprehensive serum metabolite profiling

Blood samples were coagulated (30 min, RT) and centrifuged (6,000 × g, 10 min) to obtain serum, which was cryopreserved (−80 °C) prior to processing. Metabolite extraction involved precipitation using chilled methanol (3:1 v/v methanol:serum) followed by centrifugation (15,000 × g, 15 min). The supernatant was analyzed by UPLC-Q/TOF-MS (Ekemo Tech Group, Shenzhen, China) employing an established chromatographic separation protocol [18]. Mass spectral features were processed through MarkerView 2.1 with elimination of isotopic interference and low-prevalence signals (<20% detection rate). Multivariate pattern recognition included PCA dimensionality reduction and OPLS-DA modeling (SIMCA-P v11.5), where metabolites exhibiting VIP > 1.0 with statistical significance ($p < 0.05$) underwent pathway mapping via MetaboAnalyst 3.0 and KEGG pathway interpretation to elucidate metabolic network alterations.

Statistical analysis

Quantitative data were processed using SPSS 20.0 (IBM, USA) and expressed as mean ± standard deviation. Inter-group comparisons were performed through one-way ANOVA followed by Tukey's post hoc test for multiple comparisons, with statistical significance defined as $p < 0.05$. Data visualization was implemented using GraphPad Prism (GraphPad Software Inc.) supplemented by the Bioincloud online platform (https://bioincloud.tech/) for graphical analysis.

RESULTS

Mitigation of obesity and hepatic steatosis by HF in NAFLD mice

As shown in Fig. 1, NAFLD model mice displayed significantly higher body weight and liver wet weight compared to the NC group ($p < 0.05$). HF supplementation counteracted these effects, markedly reducing both parameters relative to untreated NAFLD mice ($p < 0.05$; Fig. 1A,B).

Consistent with metabolic dysregulation, serum TC and TG levels were elevated in the NAFLD group ($p < 0.05$). While HF treatment trended toward lowering these lipids, the differences lacked statistical significance ($p > 0.05$; Fig. 1C,D). Notably, NAFLD mice developed severe insulin resistance with increased FBG, FINS, and HOMA-IR values ($p < 0.05$). HF administration significantly attenuated these abnormalities, demonstrating improved glucose homeostasis ($p < 0.05$; Fig. 1E–G).

Enhancement of systemic antioxidant defense by HF in NAFLD mice

Quantitative PCR analysis revealed substantial upregulation ($p < 0.05$) of hepatic NLRP3, Caspase-1, IL-1β, and TNF-α mRNA expression in NAFLD and HF groups compared with NC controls. HF treatment significantly downregulated Caspase-1, IL-1β, and TNF-α transcripts compared to untreated NAFLD mice ($p < 0.05$), while NLRP3 expression showed nonsignificant reduction ($p > 0.05$; Fig. 2A–D). The bile acid synthesis enzyme CYP7A1 exhibited markedly decreased hepatic expression in NAFLD mice relative to controls ($p < 0.05$), with HF administration inducing nonsignificant elevation ($p > 0.05$; Fig. 2E). Oxidative stress analysis demonstrated compromised antioxidant status in NAFLD mice, characterized by suppressed SOD and GSH-PX activities ($p < 0.05$) alongside elevated MDA concentrations compared with NC animals. Notably, HF intervention significantly restored antioxidant capacity, increasing serum SOD, GSH-PX, and T-AOC levels while reducing lipid peroxidation (MDA; $p < 0.05$ vs. NAFLD group; Fig. 2F–I). Metabolomic profiling indicated severe depletion of colonic butyrate in NAFLD mice ($p < 0.05$ compared to NC). HF supplementation effectively reversed this deficit, elevating butyrate concentrations significantly above NAFLD model levels ($p < 0.05$; Fig. 2J).

Hepatoprotective effects of HF against NAFLD pathology

Histopathological evaluation demonstrated substantial differences in liver morphology across experimental groups. In control (NC) animals, hematoxylin-eosin staining showed well-organized hepatic architecture featuring distinct lobular patterns with radially aligned sinusoids surrounding central veins (Fig. 3A). Hepatocytes maintained typical polygonal morphology with eosinophilic cytoplasm, showing neither pathological swelling nor lipid abnormalities.

NAFLD-affected livers exhibited severe structural derangement characterized by several pathological features: disruption of lobular organization, widespread cellular edema, and marked microvesicular steatosis visible as variably sized cytoplasmic vacuoles that displaced nuclei peripherally (Fig. 3B).

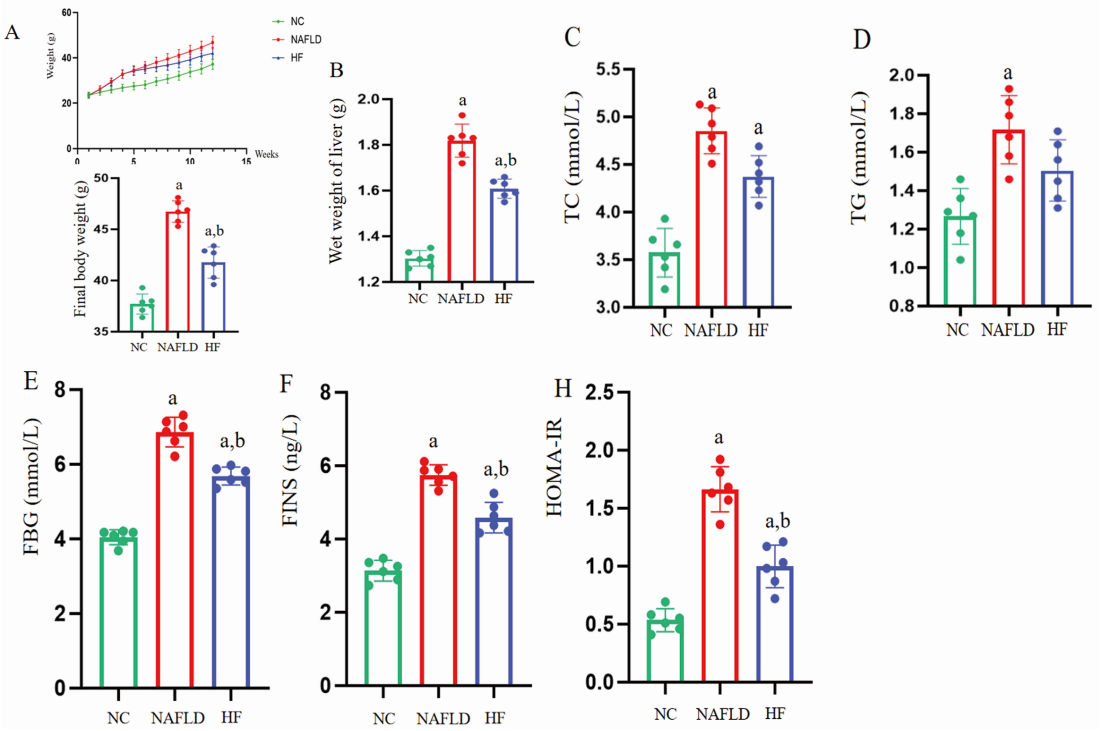

Fig. 1 Mouse body weight, liver wet weight, triglyceride, and total cholesterol levels. A: body weight; B: liver wet weight; C: triglyceride; D: total cholesterol; E: FBG; F: FINS; and G: HOMA-IR. Data are presented as the mean ± SD. Statistical significance was determined by one-way ANOVA followed by Tukey's post hoc test. a: compared with the NC group, $p < 0.05$; b: compared with the NAFLD group, $p < 0.05$.

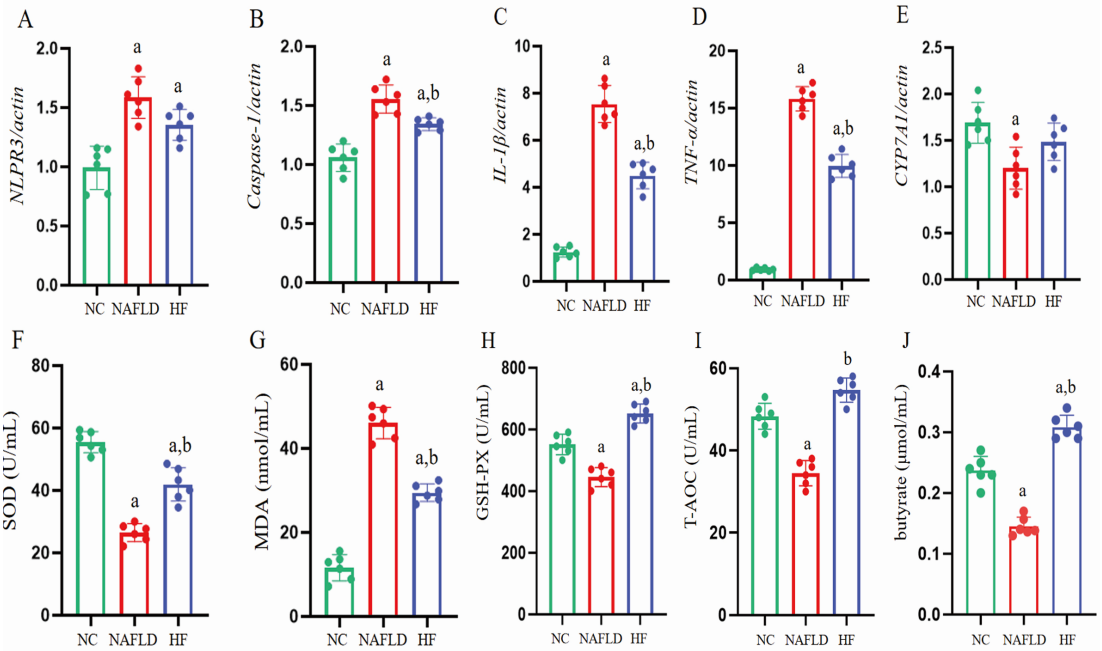

Fig. 2 Detection results of inflammation and oxidative stress levels in the liver and serum of mice. A: *NLRP3*; B: *Caspase-1*; C: *IL-1β*; D: *TNF-α*; E: *CYP7A1*; F: SOD; G: MDA; H: GSH-PX; I: T-AOC; and J: butyrate. Data are presented as the mean ± SD. Statistical significance was determined by one-way ANOVA followed by Tukey's post hoc test. a: compared with the NC group, $p < 0.05$; b: compared with the NAFLD group, $p < 0.05$.

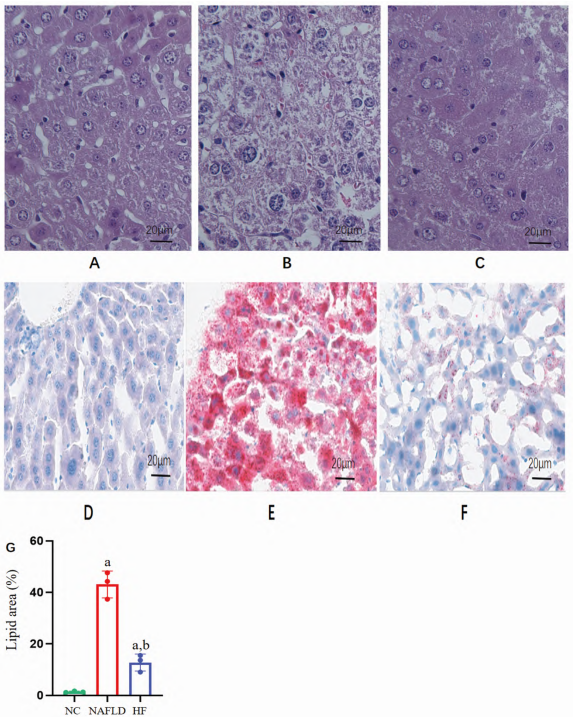

Fig. 3 Histopathological examination and quantitative analysis of lipid accumulation in mouse liver tissues. (A–C) Representative images of hematoxylin and eosin (H&E) staining of liver sections from the NC (A), NAFLD (B), and HF (C) groups. (D–F) Representative images of Oil Red O staining of liver sections from the NC (D), NAFLD (E), and HF (F) groups. Red staining indicates intracellular lipid droplets. Scale bars = 20 µm. (G) Quantitative analysis of the Oil Red O-positive area percentage (steatosis area). Data are expressed as the mean ± SD ($n = 3$). Statistical significance was determined by one-way ANOVA followed by Tukey's post hoc test. a: compared with the NC group, $p < 0.05$; b: compared with the NAFLD group, $p < 0.05$.

Additional pathological findings included multifocal necrotic areas and substantial inflammatory cell infiltration, indicative of progressive liver injury.

Therapeutic intervention with HF yielded significant histological improvements, as evidenced by attenuated hepatic steatosis and reduced cellular ballooning compared with the NAFLD group (Fig. 3B,C). Consistent with these morphological changes, quantitative analysis of Oil Red O-stained sections revealed a significant reduction in hepatic lipid accumulation. While control livers showed negligible lipid accumulation (Fig. 3D), NAFLD specimens displayed dense clusters of lipid droplets, with a lipid area percentage of 42.5 ± 5.1%. Notably, HF treatment substantially mitigated this lipid overload, reducing the lipid area to 12.3 ± 3.2% (Fig. 3F,G; $p < 0.05$ vs. NAFLD group). These data confirm the effective therapeutic potential of HF in alleviating hepatic steatosis.

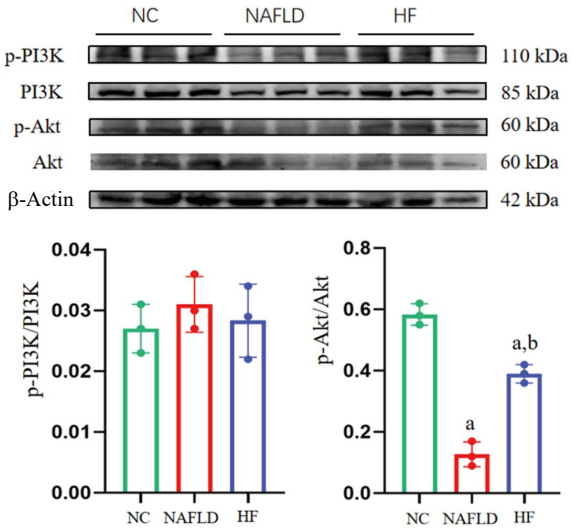

Fig. 4 Effects of HF treatment on the PI3K/Akt signaling pathway in mouse liver tissues. Representative Western blot images of phosphorylated and total PI3K and Akt (p-PI3K, PI3K, p-Akt, and Akt) are shown. β-Actin was used as a loading control. Bar graphs represent the quantitative analysis of the p-PI3K/PI3K and p-Akt/Akt ratios. Data are expressed as the mean ± SD ($n = 3$). Statistical significance was determined by one-way ANOVA followed by Tukey's post hoc test. a: $p < 0.05$ vs. the NC group; b: $p < 0.05$ vs. the NAFLD group.

Modulation of hepatic PI3K/Akt signaling pathway activation by HF

Immunoblotting analysis was performed to evaluate the activation status of the PI3K/Akt signaling pathway. First, we examined the expression levels of total proteins. As shown in Fig. 4, the levels of total PI3K and total Akt remained stable across the NC, NAFLD, and HF groups, indicating no significant alteration in protein abundance.

We then calculated the ratios of phosphorylated to total proteins to assess pathway activation. The p-PI3K/PI3K ratio showed no significant differences among the three groups ($p > 0.05$). However, significant alterations were observed in the Akt signaling axis. The p-Akt/Akt ratio was significantly suppressed in the NAFLD group compared with the NC group ($p < 0.05$). Importantly, HF administration significantly increased the p-Akt/Akt ratio compared with the untreated NAFLD mice ($p < 0.05$), partially restoring Akt phosphorylation towards normal levels. These results suggest that HF ameliorates hepatic steatosis, at least in part, by reactivating the Akt signaling cascade.

Modulation of gut microbial composition by HF in NAFLD mice

Microbiota analysis revealed distinct microbial community profiles among experimental groups. α-diversity metrics showed comparable species richness

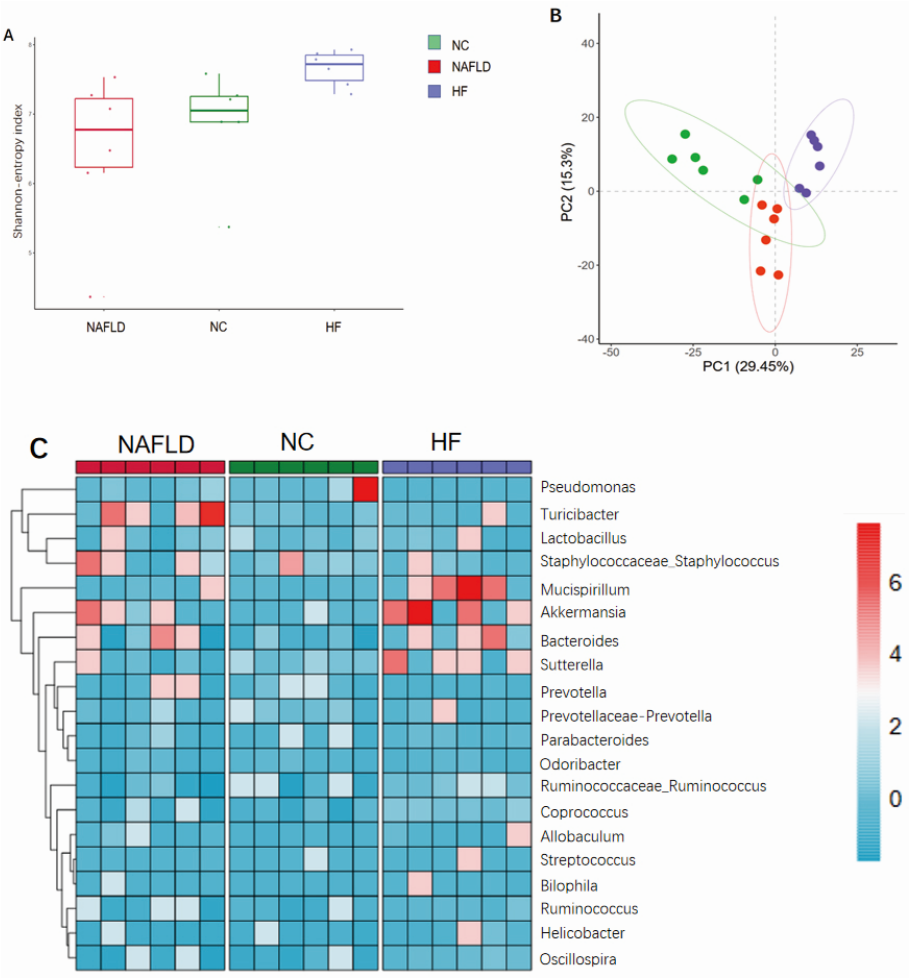

Fig. 5 Results of intestinal flora analysis in colon contents of mice. A: Intestinal flora α diversity; B: β diversity; and C: Horizontal grouped heatmap of intestinal microbiome.

across groups (Fig. 5A), whereas β-diversity analysis demonstrated significant phylogenetic segregation with clear cluster separation (Fig. 5B). Principal coordinates analysis distinctly separated HF-treated and NAFLD groups, indicating substantial microbiome restructuring following flavonoid intervention.

Taxonomic profiling identified specific genera altered by HF treatment (Fig. 5C). Compared with NAFLD controls, HF-supplemented mice showed marked enrichment of beneficial mucin-associated genera, including *Akkermansia* and *Mucispirillum*, along with elevated levels of *Bacteroides* and *Sutterella*. Conversely, the pro-inflammatory genus *Turicibacter* exhibited significant depletion in HF-treated animals.

Modulation of serum metabolic profiles and pathways by HF in NAFLD mice

Multivariate analysis of serum metabolites revealed pronounced metabolic disturbances and subsequent restoration among experimental groups. Principal component analysis (PCA) demonstrated complete separation between NC, NAFLD, and HF-treated cohorts, while orthogonal partial least squares discriminant analysis (OPLS-DA) further validated these distinctions (Fig. 6A–D). Comparative metabolomics identified significant metabolic alterations, with NAFLD mice exhibiting elevated pro-inflammatory mediators (orotidine 5′-phosphate, 3-ureidopropionate, α-D-galactose, lactose, and inosine) and depleted antioxidants (glutathione disulfide and γ-L-glutamyl-L-cysteine) relative to NC mice. HF intervention effectively counteracted these perturbations by reducing inflammatory lipids (5(S)-HETE, octadecanoic acid and 11-deoxycortisol) while enhancing cytoprotective metabolites (taurine, pyridoxamine phosphate, 1-acyl-sn-glycero-3-phosphocholine, and 3-sulfinoalanine). The list of differential metabolites can be found in Table S3 and Table S4.

Pathway enrichment analysis identified

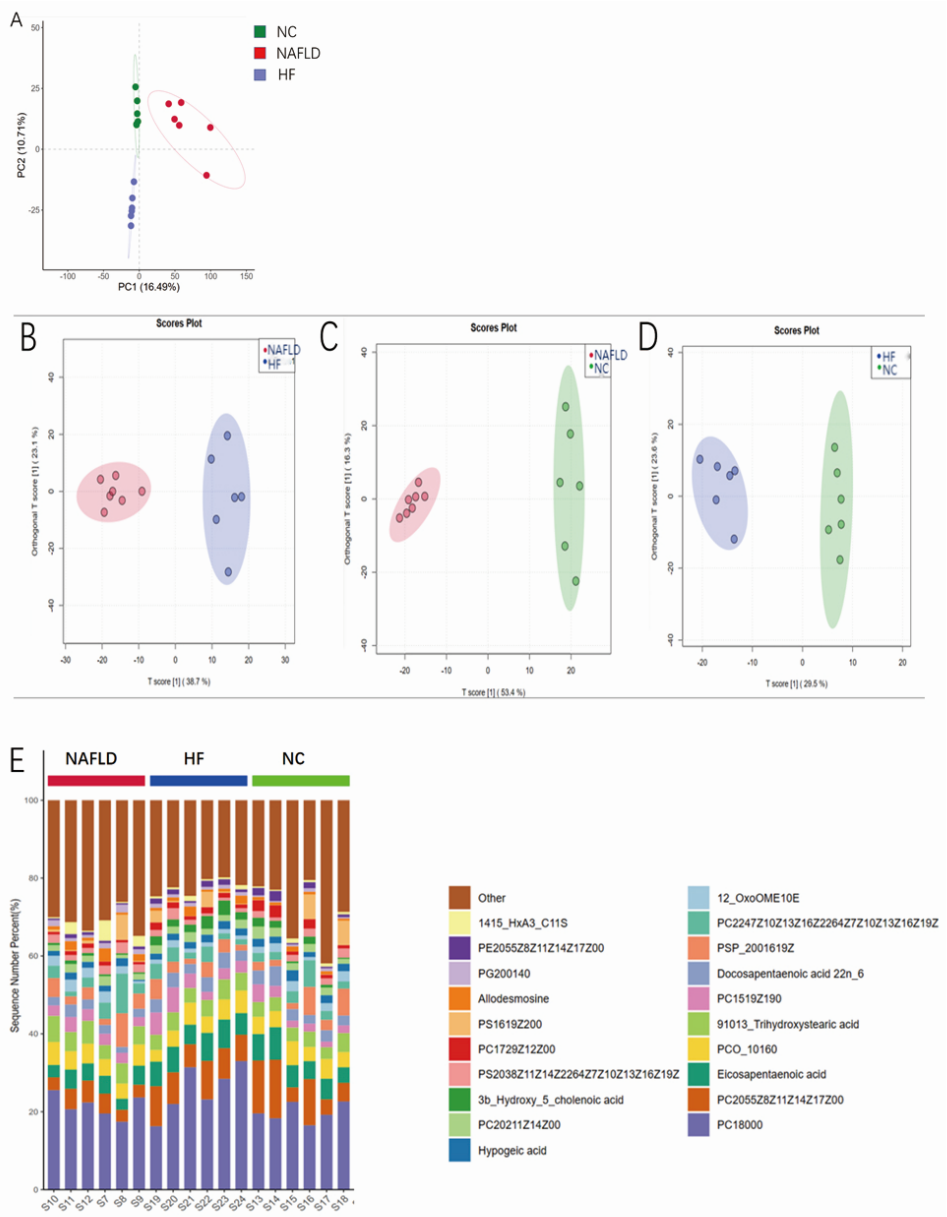

Fig. 6 Results of non-targeted metabolomics analysis in mouse serum. A: PCA scatter plot; B: PCA scatter plot of the NAFLD group vs. the HF group; C: PCA scatter plot of the NC group vs. the NAFLD group; D: PCA scatter plot of the NC group vs. the HF group; and E: Percentage stacked bar chart.

glutathione and taurine metabolism as crucial for HF-mediated oxidative stress mitigation, while glycerophospholipid metabolism and primary bile acid biosynthesis contributed to restored lipid homeostasis. Additionally, cysteine/methionine metabolism played a key role in amino acid regulation (impact score > 0.01, Fig. 7). These results collectively demonstrate that HF alleviates NAFLD-associated metabolic dysfunction through multi-pathway modulation, including redox balance restoration, anti-inflammatory effects, and improved lipid handling.

DISCUSSION

NAFLD represents a chronic hepatic disorder intricately associated with metabolic disturbances including obesity, type 2 diabetes, insulin resistance, dyslipidemia, and gut microbial dysbiosis. With escalating global prevalence and substantial healthcare burdens, NAFLD continues to pose urgent clinical challenges. Although the FDA recently approved resmetirom (Rezdiffra) as the first targeted therapy specifically for noncirrhotic NASH with moderate to

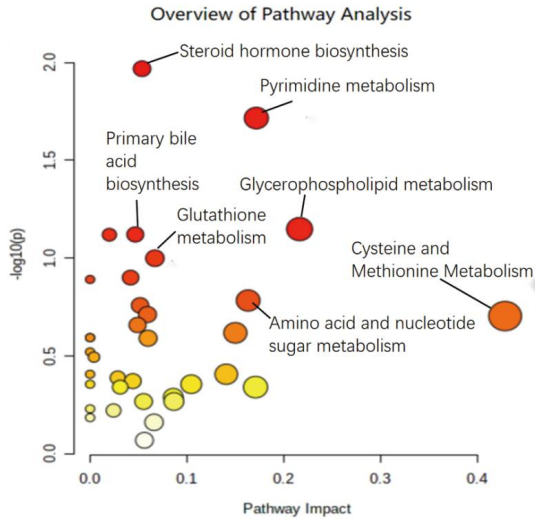

Fig. 7 Metabolic pathways regulated by Hawthorn flavonoids (HF) in the serum of NAFLD mice.

advanced fibrosis, pharmacological options for the broader spectrum of early-stage NAFLD remain limited. These circumstances underscore the ongoing critical need for identifying accessible, natural therapeutic agents with multi-target efficacy against the complex pathogenesis of NAFLD [19].

Building upon our previous investigations of probiotic interventions in diet-induced metabolic disorders, the current study evaluated the therapeutic efficacy of HF. Consistent with previous reports, HF demonstrated the capacity to significantly ameliorate hepatomegaly and reduce hepatic steatosis in NAFLD models [20]. While complete restoration of circulating lipid profiles was not the primary driver of recovery, our findings reveal the pronounced ability of HF to mitigate systemic inflammation, attenuate oxidative damage, and improve insulin signaling pathways. This suggests its therapeutic potential likely stems from multifaceted metabolic benefits rather than singular lipid-modulating effects.

Importantly, these observed mechanisms directly counteract the core drivers of NAFLD progression. Rather than reiterating the well-established "two-hit hypothesis," our results provide concrete evidence that HF effectively targets the chronic inflammation and oxidative stress cascades inherent to NAFLD. By restoring the balance between oxidation and antioxidant systems, HF appears to protect hepatocytes from oxidative metabolite-induced damage and modulate key cell signaling pathways associated with lipid peroxidation. This pharmacological profile not only aligns with Hawthorn's traditional use in metabolic disorders but also provides novel, target-specific insights into its repurposing for NAFLD management.

In our study, we found that oral administration of HF can affect various metabolic pathways related to inflammatory and oxidative stress responses in mice, including cysteine and methionine metabolism, glutathione metabolism, taurine and hypotaurine metabolism. Serum metabolomics results showed that several antioxidant metabolites in the mouse serum were significantly increased.

Compared with the NC group, the serum level of taurine in the NAFLD group mice was significantly elevated, and the level of taurine in the HF group mice was further increased compared with the NAFLD group. Taurine is an important antioxidant in the body and has therapeutic effects on NAFLD [21]. Its mechanism is to stabilize the integrity and function of the outer mitochondrial membrane to prevent liver damage, and taurine can also regulate bile acid synthesis and metabolism in the liver to intervene in the occurrence of NAFLD [22, 23].

The level of phosphonooxypyruvate (PNOP) in the serum of NAFLD mice was significantly reduced compared with the NC group. The concentration of PNOP in the serum was positively correlated with the abundance of *Akkermansia* and *Lactobacillus* in the host gut and negatively correlated with the abundance of *Bacteroides* [24]. PNOP is an intermediate product in the metabolism pathway of glycine, serine, and threonine, which can promote the metabolism of glycine, serine, and threonine to produce acetyl coenzyme A and pyruvate [25]. Moreover, acetyl coenzyme A produced by the metabolism of PNOP can also participate in the tricarboxylic acid cycle through citrate synthesis [26]. All the metabolites mentioned above were related to antioxidant stress. *Akkermansia* and *Lactobacillus* were also gut microbes associated with butyrate production. Decreased PNOP concentrations in the serum of mice with NAFLD also indicated a disturbance in their gut flora.

In the organism, orotidine 5′-phosphate can be converted into cytidine monophosphate (CMP) and uridine monophosphate (UMP) by orotate phosphoribosyltransferase and orotidine 5′-phosphate decarboxylase. An increase in the concentration of orotidine 5′-phosphate inhibits lipid oxidation in mitochondria, leading to the accumulation of lipids in liver cells [27]. The level of 3-ureidopropionate (3-UP) is significantly elevated in patients with NAFLD [28, 29]. Metabolomic profiling indicates that elevated levels of 3-UP are closely associated with impaired insulin sensitivity in patients [35]. Furthermore, mechanistic studies in metabolic disorders have demonstrated that high concentrations of 3-UP can impair mitochondrial energy homeostasis, potentially by interfering with respiratory chain and ATP synthase activities, which consequently promotes the excessive production of reactive oxygen species (ROS). This accumulation of ROS exacerbates oxidative stress and further drives insulin resistance [30]. Pyridoxamine phosphate (PP) is also an endogenous antioxidant. Aspartate transaminase is

an important metabolic enzyme in the liver, and PP acts as a coenzyme for aspartate transaminase, playing a role in amino transfer reactions [31]. In NAFLD, PP is consumed and reduced, but supplementation with exogenous PP can be used to treat NAFLD [32].

In this study, we observed a significant modulation of glutathione disulfide (GSSG) concentrations in the serum of NAFLD mice following HF treatment. The pathogenesis of NAFLD is currently best understood through the "multiple-hit hypothesis", which emphasizes a complex interplay of various factors, including insulin resistance, oxidative stress, and crucially, gut microbiota dysbiosis communicating via the gut-liver axis [33]. In this model, altered gut microbiota and increased intestinal permeability deliver endotoxins and disruptive metabolites to the liver, synergizing with an increase in ROS. This combined assault leads to lipid peroxidation, hepatocyte damage, excessive inflammatory responses, and liver fibrosis driven by hepatic stellate cell activation. The excessive accumulation of GSSG reflects a severe disruption of the intracellular redox balance caused by these multiple hits. This prominent oxidative stress environment impairs insulin signaling pathways—primarily through the activation of stress-sensitive kinases—thereby inducing insulin resistance, which further exacerbates liver fat accumulation and necroinflammation [34]. During this process, antioxidants that protect the liver from ROS damage and lipid peroxidation are depleted, leading to a significant reduction in antioxidants such as reduced glutathione, vitamin E, and vitamin C, as frequently observed in patients with NASH. Our findings suggest that HF effectively intervenes in this multiple-hit cascade by modulating the gut microbiota and mitigating the subsequent oxidative burden on the liver.

We also found that the level of phosphatidylethanolamine (PE) in the serum of NAFLD mice significantly decreased after treatment with HF. There is currently limited research on the role of phospholipid metabolism in NAFLD, but existing studies suggest that an increase in PE levels is associated with the development of NAFLD [35]. *In vitro* studies have shown that PE can significantly inhibit cell proliferation, reduce mitochondrial membrane potential, induce lipid accumulation, and generate ROS within the mitochondria. Supplementing with exogenous phosphatidylcholine also contributes to the treatment of NAFLD.

Insulin resistance is closely related to the occurrence of NAFLD. Previous research results have shown that insulin resistance can induce lipid metabolism abnormalities, leading to excessive fat deposition in the liver, further inducing oxidative stress and lipid peroxidation in the liver, ultimately leading to NAFLD. The PI3K/Akt signaling pathway is the main signaling pathway for insulin action and is expected to become a target for improving NAFLD [36]. In this study, we observed a differential regulation within this pathway in the liver tissue of mice treated with HF. Specifically, while the phosphorylation levels of PI3K were not significantly altered, the activation of Akt was significantly enhanced compared with NAFLD mice. This divergence suggests that HF may not directly activate upstream PI3K but rather modulates targets downstream of PI3K or parallel signaling molecules that converge on Akt. This distinct targeted mechanism differs from other natural plant extracts; for example, the diarylheptanoid DPHD from *Curcuma comosa* has been shown to alleviate TNF-a-induced insulin resistance by directly upregulating both upstream phosphorylated PI3K and phosphorylated Akt [36]. For instance, HF might exert its effects by inhibiting negative regulators of Akt (such as PTEN or specific phosphatases) or by modulating other Akt-activating kinases (such as mTORC2). Through this targeted enhancement of Akt activation, HF plays a crucial anti-inflammatory and antioxidant stress role, thereby ameliorating hepatic lipid metabolism abnormalities.

Existing studies mainly focus on the direct effects of HF on the liver, exerting anti-inflammatory and antioxidant effects, while paying little attention to the improvement effect of HF on the gut microbiota of NAFLD animal models or patients. Our gut microbiota sequencing study found that HF can increase the abundance of *Mucispirillum*, *Akkermansia*, *Bacteroides*, and *Sutterella* in the intestines of NAFLD mice. Research has shown that the above-mentioned gut microbiota can ferment dietary fibers and resistant starches that humans cannot digest, producing short-chain fatty acids (SCFA) [37]. SCFA are organic acids with fewer than six carbon atoms that are beneficial to human health. The main SCFA in the human gut are acetic acid, propionic acid, and butyric acid, with butyric acid having the most significant anti-inflammatory and antioxidant functions. Through further analysis using UPLC-MS/MS technology, we found that the concentration of butyric acid in the intestines of NAFLD mice treated with HF was significantly increased.

Numerous studies have shown that an increase in specific gut bacteria, such as *Akkermansia* and *Bacteroides*, can significantly enhance colonic butyrate production, primarily through microbial cross-feeding networks where their metabolic byproducts (e.g., acetate) are utilized by true butyrate producers [38, 39]. Currently, there is limited research on the therapeutic effects of butyrate on NAFLD. Existing studies have found that butyrate can regulate appetite, increase energy expenditure, and improve insulin resistance [40]. Furthermore, mechanistic studies have explicitly demonstrated that butyrate salts can activate the PI3K/Akt signaling pathway, thereby mitigating cellular oxidative stress and exerting potent antioxidant effects [41]. In this study, after treatment with HF, NAFLD mice showed a significant increase in the

production of butyrate in the colon. Based on these results, we speculate that another important potential mechanism of HF in treating NAFLD is by regulating the gut microbiota to increase butyrate production, which then enters the liver through the bloodstream to exert anti-inflammatory and antioxidant stress effects.

Finally, it is important to acknowledge the limitations associated with using a commercially prepared HF extract. Because the exact extraction and purification protocols of the manufacturer are proprietary and not fully disclosed, the complete phytochemical profile and its exact reproducibility may be restricted. However, the HF used in this study was standardized for a high flavonoid content (⩾60%). While our HPLC-DAD-MS analysis identified specific constituents—such as hyperoside, vitexin, rutin, and epicatechin—these compounds possess distinct chemical properties and potentially different biological effects on liver metabolism and pathology. In the absence of compound-specific dosing or mechanistic analyses, attributing the observed hepatic effects broadly to "flavonoids" may be an overgeneralization. Therefore, the outcomes observed in this study should be interpreted as the synergistic effects of a flavonoid-rich mixture. Furthermore, since the concentration of residual components was not quantified in our laboratory, we cannot entirely rule out the possibility that trace polysaccharides or other phytochemicals might exert a minor synergistic prebiotic-like effect on gut microbiota modulation. Future mechanistic studies utilizing highly purified flavonoid monomers or fully characterized, in-house extracted fractions are warranted to further isolate and confirm the specific active compounds responsible for the observed therapeutic effects.

CONCLUSION

In summary, our findings demonstrate that HF exerts a therapeutic effect on NAFLD mice by directly regulating oxidative stress-related pathways, particularly the glutathione and taurine metabolism pathways. Furthermore, HF modulates the gut microbiota, leading to an enrichment of beneficial metabolites such as butyrate. Acting via the 'gut-liver axis', butyrate mitigates hepatic oxidative stress. Crucially, this protective response is mechanistically driven by the specific enhancement of Akt activation independent of upstream PI3K phosphorylation, rather than a uniform activation of the classical PI3K/Akt cascade.

Appendix A. Supplementary data

Supplementary data associated with this article can be found at https://dx.doi.org/10.2306/scienceasia1513-1874.2026.037. The data that support the findings of this study are available from the corresponding author upon reasonable request.

Acknowledgements: This research was funded by Yancheng Municipal Health Commission Medical Research Project (YK2023142) and Jurong Social Development Science and Technology Program Project (Grant No. ZA42306). The authors would like to thank Assoc. Prof. Shi Yingjuan from the School of Foreign Languages, Jiangsu University, for her assistance in language and grammar during the preparation of this manuscript.

REFERENCES

1. Abdelmalek MF (2021) Nonalcoholic fatty liver disease: Another leap forward. *Nat Rev Gastroenterol Hepatol* **18**, 85–86.
2. Zhou J, Zhou F, Wang W, Zhang X, Ji Y, Zhang P, She Z, Zhu L, et al (2020) Epidemiological features of NAFLD from 1999 to 2018 in China. *Hepatology* **71**, 1851–1864.
3. Palma R, Pronio A, Romeo M, Scognamiglio F, Ventriglia L, Ormando VM, Lamazza A, Pontone S, et al (2022) The role of insulin resistance in fueling NAFLD pathogenesis: From molecular mechanisms to clinical implications. *J Clin Med* **11**, 3649.
4. Xu S, Chen Y, Miao J, Li Y, Liu J, Zhang J, Liang J, Chen S, et al (2024) Esculin inhibits hepatic stellate cell activation and CCl_4-induced liver fibrosis by activating the Nrf2/GPX4 signaling pathway. *Phytomedicine* **128**, 155465.
5. Monti E, Vianello C, Leoni I, Galvani G, Lippolis A, D'Amico F, Roggiani S, Stefanelli C, et al (2025) Gut microbiome modulation in hepatocellular carcinoma: Preventive role in NAFLD/NASH progression and potential applications in immunotherapy-based strategies. *Cells* **14**, 84.
6. Song Y, Liu S, Zhang L, Zhao W, Qin Y, Liu M (2024) The effect of gut microbiome-targeted therapies in nonalcoholic fatty liver disease: A systematic review and network meta-analysis. *Front Nutr* **11**, 1470185.
7. Jurikova T, Sochor J, Rop O, Mlcek J, Balla S, Szekeres L, Adam V, Kizek R (2012) Polyphenolic profile and biological activity of Chinese hawthorn (*Crataegus pinnatifida* BUNGE) fruits. *Molecules* **17**, 14490–14509.
8. Liu Z, Gao T, Chang H, Xu Y, Wang L, Wang X, Lang J, Yu Y, et al (2025) Hawthorn leaf and its extract alleviate high-fat diet-induced obesity and modulate gut microbiome in mice. *Curr Res Food Sci* **10**, 101025.
9. Wang T, Wang D, Ding Y, Xu H, Sun Y, Hou J, Zhang Y (2024) Targeting non-alcoholic fatty liver disease with Hawthorn ethanol extract (HEE): A comprehensive examination of hepatic lipid reduction and gut microbiota modulation. *Nutrients* **16**, 1335.
10. Zhu L, Li S, Zheng W, Ni W, Cai M, Liu H (2023) Targeted modulation of gut microbiota by traditional Chinese medicine and natural products for liver disease therapy. *Front Immunol* **14**, 1086078.
11. Zhang Y, Sun J, Zhang X, Zhong Q, Hao P, Yin W, Chen B, Wei Q, et al (2025) Structural characterisation of hawthorn polysaccharide and its mechanisms of action against non-alcoholic fatty liver disease. *Int J Biol Macromol* **319**, 145713.
12. Hu H, Weng J, Cui C, Tang F, Yu M, Zhou Y, Shao F, Zhu Y (2022) The hypolipidemic effect of Hawthorn leaf flavonoids through modulating lipid metabolism and gut microbiota in hyperlipidemic rats. *Evid Based Complement Alternat Med* **2022**, 3033311.
13. Li D, Li Y, Yang S, Zhang X, Cao Y, Zhao R, Zhao Y, Jin X, et al (2025) Polydatin combined with hawthorn

flavonoids alleviate high fat diet induced atherosclerosis by remodeling the gut microbiota and glycolipid metabolism. *Front Pharmacol* **16**, 1515485.
14. Preguiça I, Alves A, Nunes S, Fernandes R, Gomes P, Viana SD, Reis F (2020) Diet-induced rodent models of obesity-related metabolic disorders: A guide to a translational perspective. *Obes Rev* **21**, e13081.
15. Li Z, Xu J, Zheng P, Xing L, Shen H, Yang L, Zhang L, Ji G (2015) Hawthorn leaf flavonoids alleviate nonalcoholic fatty liver disease by enhancing the adiponectin/AMPK pathway. *Int J Clin Exp Med* **8**, 17295–17307.
16. He J, Li X, Yan M, Chen X, Sun C, Tan J, Song Y, Xu H, et al (2024) Inulin reduces kidney damage in Type 2 diabetic mice by decreasing inflammation and serum metabolomics. *J Diabetes Res* **2024**, 1222395.
17. Bolyen E, Rideout JR, Dillon MR, Bokulich NA, Abnet CC, Al-Ghalith GA, Alexander H, Alm EJ, et al (2019) Reproducible, interactive, scalable and extensible microbiome data science using QIIME 2. *Nat Biotechnol* **37**, 852–857.
18. Want EJ, Wilson ID, Gika H, Theodoridis G, Plumb RS, Shockcor J, Holmes E, Nicholson JK (2010) Global metabolic profiling procedures for urine using UPLC-MS. *Nat Protoc* **5**, 1005–1018.
19. Harrison SA, Bedossa P, Guy CD, Schattenberg JM, Loomba R, Taub R, Labriola D, Moussa SE, et al (2024) A phase 3, randomized, controlled trial of Resmetirom in NASH with liver fibrosis. *N Engl J Med* **390**, 497–509.
20. Zheng L, Lu Z, Ma Y, Cui P, Zhang X, Gan J, Li G (2025) Hawthorn total flavonoids ameliorate hyperlipidemia through AMPK/SREBP1-c and PPARα/PGC-1α/CPT-1A pathway activation and gut microbiota modulation. *J Sci Food Agric* **105**, 4326–4337.
21. Haidari F, Asadi M, Mohammadi-Asl J, Ahmadi-Angali K (2020) Effect of weight-loss diet combined with taurine supplementation on body composition and some biochemical markers in obese women: A randomized clinical trial. *Amino Acids* **52**, 1115–1124.
22. San J, Hu J, Pang H, Zuo W, Su N, Guo Z, Wu G, Yang J (2023) Taurine protects against the fatty liver hemorrhagic syndrome in laying hens through the regulation of mitochondrial homeostasis. *Int J Mol Sci* **24**, 10360.
23. Naito Y, Ushiroda C, Mizushima K, Inoue R, Yasukawa Z, Abe A, Takagi T (2020) Epigallocatechin-3-gallate (EGCG) attenuates non-alcoholic fatty liver disease via modulating the interaction between gut microbiota and bile acids. *J Clin Biochem Nutr* **67**, 2–9.
24. He F, Jin X, Wang C, Hu J, Su S, Zhao L, Geng T, Zhao Y, et al (2023) Lactobacillus rhamnosus GG ATCC53103 and Lactobacillus plantarum JL01 improved nitrogen metabolism in weaned piglets by regulating the intestinal flora structure and portal vein metabolites. *Front Microbiol* **14**, 1200594.
25. Cheng ZX, Guo C, Chen ZG, Yang TC, Zhang JY, Wang J, Zhu JX, Li D, et al (2019) Glycine, serine and threonine metabolism confounds efficacy of complement-mediated killing. *Nat Commun* **10**, 3325.
26. Gonzalez-Rellan MJ, Fernández U, Parracho T, Novoa E, Fondevila MF, da Silva Lima N, Ramos L, Rodríguez A, et al (2023) Neddylation of phosphoenolpyruvate carboxykinase 1 controls glucose metabolism. *Cell Metab* **35**, 1630–1645.e5.
27. Matilainen J, Mustonen AM, Rilla K, Käkelä R, Sihvo SP, Nieminen P (2020) Orotic acid-treated hepatocellular carcinoma cells resist steatosis by modification of fatty acid metabolism. *Lipids Health Dis* **19**, 70.
28. Stefanakis K, Mingrone G, George J, Mantzoros CS (2025) Accurate non-invasive detection of MASH with fibrosis F2-F3 using a lightweight machine learning model with minimal clinical and metabolomic variables. *Metabolism* **163**, 156082.
29. Luukkonen PK, Sakuma I, Gaspar RC, Mooring M, Nasiri A, Kahn M, Zhang XM, Zhang D, et al (2023) Inhibition of HSD17B13 protects against liver fibrosis by inhibition of pyrimidine catabolism in nonalcoholic steatohepatitis. *Proc Natl Acad Sci USA* **120**, e2217543120.
30. Kölker S, Okun JG, Hörster F, Assmann B, Ahlemeyer B, Kohlmüller D, Exner-Camps S, Mayatepek E, et al (2001) 3-Ureidopropionate contributes to the neuropathology of 3-ureidopropionase deficiency and severe propionic aciduria: a hypothesis. *J Neurosci Res* **66**, 666–673.
31. Han M, Zhang C, Suglo P, Sun S, Wang M, Su T (2021) l-Aspartate: An essential metabolite for plant growth and stress acclimation. *Molecules* **26**, 1887.
32. Kobayashi T, Kessoku T, Ozaki A, Iwaki M, Honda Y, Ogawa Y, Imajo K, Yoneda M, et al (2021) Vitamin B6 efficacy in the treatment of nonalcoholic fatty liver disease: An open-label, single-arm, single-center trial. *J Clin Biochem Nutr* **68**, 181–186.
33. Tilg H, Moschen AR (2010) Evolution of inflammation in nonalcoholic fatty liver disease: The multiple parallel hits hypothesis. *Hepatology* **52**, 1836–1846.
34. Chen Z, Tian R, She Z, Cai J, Li H (2020) Role of oxidative stress in the pathogenesis of nonalcoholic fatty liver disease. *Free Radic Biol Med* **152**, 116–141.
35. Shama S, Jang H, Wang X, Zhang Y, Shahin NN, Motawi TK, Kim S, Gawrieh S, et al (2023) Phosphatidylethanolamines are associated with nonalcoholic fatty liver disease (NAFLD) in obese adults and induce liver cell metabolic perturbations and hepatic stellate cell activation. *Int J Mol Sci* **24**, 1034.
36. Charaslertrangsi T, Yanukun K, Suksamrarn A, Piyachaturawat P, Sutjarit N (2025) Suppression of TNF-α-induced dysregulation of adipocytokine and insulin signaling in 3T3-L1 adipocytes by a diarylheptanoid from Curcuma comosa. *ScienceAsia* **51**, ID 2025040.
37. Markowiak-Kopeć P, Śliżewska K (2020) The effect of probiotics on the production of short-chain fatty acids by human intestinal microbiome. *Nutrients* **12**, 1107.
38. Belzer C, Chia LW, Aalvink S, Chamlagain B, Piironen V, Knol J, de Vos WM (2017) Microbial metabolic networks at the mucus layer lead to diet-independent butyrate and vitamin B12 production by intestinal symbionts. *mBio* **8**, e00770-17.
39. Chia LW, Mank M, Blijenberg B, Aalvink S, Bongers RS, Stahl B, Knol J, Belzer C (2020) Bacteroides thetaiotaomicron fosters the growth of butyrate-producing anaerostipes caccae in the presence of lactose and total human milk aarbohydrates. *Microorganisms* **8**, 1513.
40. Canfora EE, Meex R, Venema K, Blaak EE (2019) Gut microbial metabolites in obesity, NAFLD and T2DM. *Nat Rev Endocrinol* **15**, 261–273.
41. Tang G, Du Y, Guan H, Jia J, Zhu N, Shi Y, Rong S, Yuan W (2022) Butyrate ameliorates skeletal muscle atrophy in diabetic nephropathy by enhancing gut barrier function and FFA2-mediated PI3K/Akt/mTOR signals. *Br J Pharmacol* **179**, 159–178.

Appendix A. Supplementary data

Table S1 qRT-PCR primer sequences.

Gene	Primer sequence (5′ → 3′)
Mouse_acin	F: CATCACTGCCACCCAGAAGACTG R: ATGCCAGTGAGCTTCCCGTTCAG
*Mouse_IL-1*β	F: CCTGTCCTGCGTGTTGAAAGA R: GGGAACTGGGCAGACTCAAA
*Mouse_TNF-*α	F: AATGGCGTGGAGCTGAGA R: TGGCAGAGAGGAGGTTGAC
Mouse_NLRP3	F: AACAGCCACCTCACTTCCAG R: CCAACCACAATCTCCGAATG
Mouse_Caspase-1	F: GCACAAGACCTCTGACAGCA R: TTGGGCAGTTCTTGGTATTC
Mouse_CPY7A1	F: CAGGCTGACTCTGAACTTGC R: AGACCAAGAGCTGATGCAGT

Table S2 Detailed specifications, catalog numbers, and Research Resource Identifiers (RRIDs) of antibodies used in this study.

Antibody name	Manufacturer	Cat. No.	RRID
β-actin	Proteintech	60008-1-Ig	RRID:AB_2289225
Akt (Total)	Proteintech	60225-1-Ig	RRID:AB_2289225
p-Akt (Ser473)	Proteintech	66444-1-Ig	RRID:AB_2289225
PI3K p85	Proteintech	18940-1-AP	RRID:AB_2289225
p-PI3K	Proteintech	66225-1-Ig	RRID:AB_2289225
HRP	Beyotime	A0208	N/A

Table S3 Differential metabolites between the NC group and the NAFLD group.

No	Metabolite	HMDB	m/z	Retention time (min)	Vs. NC group
1	Adenosyl-L-methionine	HMDB0000218	399.44	12.39	↑
2	Phosphonooxypyruvate	HMDB0001227	84.23	14.99	↓
3	Finylpyruvate	HMDB0001274	152.16	11.07	↓
4	Ophthalmate	HMDB0000206	222.23	10.26	↑
5	Orotidine 5′-phosphate	HMDB0000143	322.18	12.39	↑
6	dTMP	HMDB0003556	402.20	14.99	↓
7	dTDP	HMDB0001265	135.75	7.52	↓
8	3-Ureidopropionate	HMDB0001274	102.27	6.95	↑
9	alpha-D-Galactose	HMDB0000143	545.26	16.99	↑
10	L-Fucose 1-phosphate	HMDB0001265	401.95	14.78	↓
11	Lactose	HMDB0041627	125.36	6.81	↑
12	alpha-D-Galactose	HMDB0000143	176.88	8.91	↑
13	Glutathione disulfide	HMDB0003337	295.33	12.39	↓
14	Gamma-L-Glutamyl-L-cysteine	HMDB0001049	389.65	14.19	↓
15	1D-myo-Inositol	HMDB0001143	433.26	15.09	↓
16	D-Glyceraldehyde -phosphate	HMDB0001112	289.36	12.38	↑
17	Taurine	HMDB0000251	249.65	11.36	↑
18	Xanthine	HMDB0000292	126.26	8.90	↑
19	Inosine	HMDB0000195	216.88	11.51	↑
20	5′-Phosphoribosyl-N-formylglycinamide	HMDB0001308	314.18	9.65	↑

Table S4 Differential metabolites between the NAFLD group and the HF group.

No	Metabolite	HMDB	m/z	Retention time (min)	Vs. NAFLD group
1	Taurine	HMDB0000251	599.23	15.03	↑
2	3alpha,7alpha,12alpha-Trihydroxy-5beta-cholestan-26-al	HMDB0012458	446.35	12.29	↓
3	7alpha-Hydroxy-3-oxo-4-cholestenoate	HMDB0012564	547.02	14.25	↓
4	Pyridoxamine phosphate	HMDB0001555	423.21	11.07	↑
5	Biotinyl-5′-AMP	HMDB0004220	399.12	10.26	↑
6	Phosphatidylcholine	HMDB000299	459.23	12.45	↑
7	Xanthosine	HMDB000299	583.07	14.36	↓
8	5(S)-HETE	HMDB0011134	369.39	7.52	↓
9	Octadecanoic acid	HMDB0000827	343.12	6.95	↓
10	PC(16:0/0:0)	HMDB0010382	530.30	14.29	↓
11	(5Z,8Z,11Z,14Z,17Z)-Icosapentaenoic acid	HMDB0001999	450.51	12.39	↓
12	Cortisol	HMDB0000063	603.15	14.99	↑
13	Androsterone	HMDB0000031	332.56	6.81	↓
14	Estrone 3-sulfate	HMDB0001425	370.24	8.91	↓
15	Pregnanolone	HMDB0001449	450.36	12.39	↑
16	11-Deoxycortisol	HMDB0000015	589.45	14.99	↓
17	Phosphatidylethanolamine	HMDB0000725	609.23	15.09	↓
18	Phosphatidylcholine	HMDB0000571	450.79	12.38	↓
19	1-Acyl-sn-glycero-3-phosphocholine	HMDB0000479	430.07	11.36	↑
20	3-Sulfinoalanine	HMDB0000996	363.02	8.90	↑